PERGAMON

International Journal of Solids and Structures 40 (2003) 7197–7217

INTERNATIONAL JOURNAL OF SOLIDS and STRUCTURES

www.elsevier.com/locate/ijsolstr

Size effect and asymptotic matching analysis of fracture of closed-cell polymeric foam

Zdeněk P. Bažant [a,*], Yong Zhou [b], Goangseup Zi [b], Isaac M. Daniel [c]

[a] *Departments of Civil Engineering and Materials Science, Northwestern University, 2145 Sheridan Road, Tech-CEE, Evanston, IL 60208, USA*

[b] *Department of Civil Engineering, Northwestern University, Evanston, IL 60208, USA*

[c] *Departments of Civil and Mechanical Engineering, Northwestern University, Evanston, IL 60208, USA*

Received 3 December 2002

Abstract

The effect of structure size on the nominal strength of closed-cell PVC foam (Divinycell H100) is investigated experimentally, theoretically and numerically. Two types of size effect are considered—Type I, characterizing failure of structures with large cracks or notches, and Type II, characterizing failure at crack initiation. Geometrically similar single edge-notched prismatic specimens of cross section widths 6.35, 43.9 and 305 mm, are tested under tension. The results are shown to agree with Bažant's law for type I energetic (deterministic) size effect derived by asymptotic matching of a solution by equivalent linear elastic fracture mechanics for large sizes and plastic crack solution for small sizes (in the derivation, the statically indeterminate size-dependent lateral shift of the axial load resultant due to rotational end restrain is taken into account). Fitting this law, previously verified for many quasibrittle materials, to the test results furnishes the values of the fracture energy of the foam as well as the characteristic size of the fracture process zone of foam. The size effect method of measuring the fracture characteristics of foam is further supported by analysis of recent notched beam tests of Zenkert and Bäcklund. Furthermore, it is shown that compressed V-notched specimens exhibit no size effect. Subsequently, the size effect of Type II is studied using previous test data of Fleck, Olurin and coworkers for dissimilar long holed panels having different width and different diameter-width ratios. An asymptotic matching formula for this type of size effect (similar to a previously derived formula for kink band failure of fiber composites) is set up and is shown capable of matching the test data well. But its verification as a predictive tool cannot yet be claimed because of inaccurate asymptotic properties of the available energy release function. Finally, the size effect of Type I is analyzed using the eigenvalue method for the cohesive crack model and the numerical results are shown to agree again with both Bažant's size effect law and the test results.

1. Introduction

Because of their very high stiffness-weight and strength-weight ratios, good thermal insulation, high energy absorption and other advantages, the use of sandwich structures in aircraft, ship building and

* Corresponding author. Tel.: +1-847-491-4025; fax: +1-847-491-3741.
E-mail address: z-bazant@northwestern.edu (Z.P. Bažant).

0020-7683/$ - see front matter © 2003 Elsevier Ltd. All rights reserved.
doi:10.1016/S0020-7683(03)00362-7

mechanical engineering is increasing. The cores of sandwich plates are often light cellular materials such as a closed-cell rigid polymeric foam made from polyvinyl chloride (PVC), polystyrene (PS) or polyurethane (PUR).

Sandwich structures have been investigated systematically since the 1950s. Several basic mechanisms of failure have been identified (e.g., Triantafillou and Gibson, 1987; Gibson and Ashby, 1997). The skins may fail by buckling delamination with fracture or by buckling triggered by prior indentation. They may also fail by quasiplastic extension with distributed damage, or by compressive or tensile fracture of the skin. The core may fail by plastic deformation or by fracture. The overall failure may be triggered by any one of these mechanisms, and a complete failure typically involves a combination of failures in both the core and the skins.

A difficult aspect of sandwich failure is the development of distributed damage and its localization. This phenomenon has been shown to cause large deterministic size effects in other quasibrittle materials, and by analogy the same must be expected for sandwich structures. With this motivation, a microplane constitutive model for a rigid closed-cell polymeric foam and a finite element model for the nonlinear deformations of a sandwich plate have been developed at Northwestern University (Bažant and Brocca, 2000; Brocca et al., 2001). The computed load–deflection curves of a sandwich beam were found to exhibit a distinct deterministic size effect.

The present paper deals with a closed-cell vinyl foam. In classical works, the failure of this material in tension or compression has usually been described as ductile, involving a yield plateau followed by locking, and failure criteria expressed in terms of stresses have been used (e.g., Gibson and Ashby, 1997; Shipsha et al., 2000; Gdoutos et al., 2001). This kind of failure can exhibit no size effect.

Such ductile response, however, does not take place when high tensile stress concentrations exist, induced for example by notches in laboratory specimens, or various structural holes or accidental damage of real structures. In such a case, the failure of the foam may be brittle, as revealed most clearly by the notched specimen tests of Zenkert (1989) and Zenkert and Bäcklund (1989) (and partly also suggested by holed panel tests of Olurin et al. (2001) and Fleck et al. (2001)). The brittle failure must generally be expected to exhibit a pronounced size effect (Bažant and Planas, 1998; Bažant, 2002). A size effect was revealed already in 1989 by Zenkert and Bäcklund's tests of notched foam beams.

However, the size effect in foam, which is important for extrapolating laboratory test data to very large structures such as large ships, has not been adequately explored. Especially, the size effect in foam has not been described analytically by simple formulae which would be easily usable in design and which could be exploited for convenient identification of material fracture properties from the measured size effect on the load capacities of notched foam specimens. To present such analytical formulae is the objective of the present study.

This objective is made easy by analogy with previous studies of the size effects in quasibrittle materials. This paper will explore whether the energetic size effect law for quasibrittle failure of structures with large cracks, proposed by Bažant (1984), extended by Bažant and Kazemi (1990), and verified for concrete, rocks, sea ice, ceramics, fiber composites and other quasibrittle materials (Bažant and Planas, 1998; Bažant, 2002), can be applied to rigid polymeric foam and used for material parameter identification. The law of size effect for failures at fracture initiation will be also studied.

2. Experimental setup, fracture tests and results

Fracture was tested on PVC (Divinycell H100) foam with nominal density 100 kg/m^3, which is closed-cell rigid foam widely used for sandwich cores. All the specimens were cut from one and the same plate (supplied by Diab Inc., DeSoto, Texas) and had the same thickness $b = 25.40$ mm. To determine the size effect in tensile (model I) fracture, specimens geometrically similar in two dimensions with length-to-width ratio 5:2 were selected. Their widths were $D = 6.35$, 43.94 and 304.80 mm (Fig. 1). Notches of width 1.00

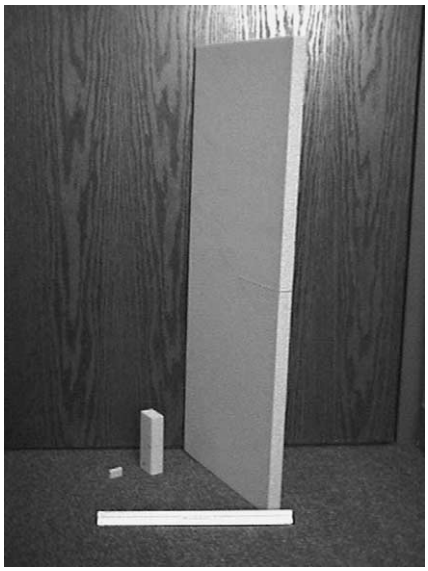

Fig. 1. Foam specimens geometrically similar in two dimensions for tensile fracture test (Divinycell H100).

mm and depth $0.4D$ were cut with a band saw. The tip of the notch was sharpened by a blade having the thickness of 0.25 mm.

In addition, compressive tests were carried out using the same specimens but only of the middle size. To avoid the opposite faces of the notch from getting in contact before the maximum compressive load is reached, the notch was widened with a band saw to a wedge shape of width 25 mm at the notch mouth. The notch tip was sharpened by a razor blade. The ends of specimens were glued by epoxy to very stiff steel platens which were gripped in the loading machine, with any rotation of the ends prevented.

The specimens were loaded in tension in a closed-loop testing machine (Instron-8500) (Fig. 2). To minimize the viscoelastic effects due to differences in the loading rate, the displacement rate of the platens

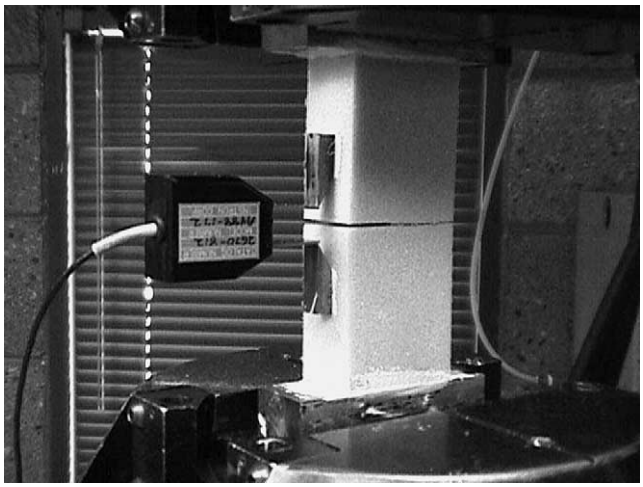

Fig. 2. Test set-up for a median size specimen in tensile fracture test.

was uniform throughout the test and was chosen such that the specimens of any size would reach the maximum load within about 5 min. The displacements were measured by LVDT gages mounted across the notch mouth (Fig. 2) spanning, in the case of tension tests, a base length of 11.50 mm. The geometries and peak loads for all the tensile and compressive specimens are listed in Table 1, and the typical load–displacement curves are shown in Fig. 3.

The choice of the test specimen and loading setup was guided by the following two considerations:

1. One reason for cutting notches was to ensure the failure to begin at one desired place. Otherwise, the failure could start at diverse locations where the material is statistically the weakest, which could cause

Table 1
Specimen dimensions and experimental results

	No.	b (mm)	D (mm)	L (mm)	P (N)	σ_N (MPa)
Small tensile specimens	1	25.40	6.35	15.88	241.09	1.49
	2	25.40	6.35	15.88	205.60	1.27
	3	25.40	6.35	15.88	249.99	1.55
	4	25.40	6.35	15.88	246.43	1.53
	5	25.40	6.35	15.88	237.27	1.47
	6	25.40	6.35	15.88	204.30	1.27
Medium tensile specimens	1	25.40	43.94	109.85	739.29	0.68
	2	25.40	43.94	109.85	662.34	0.61
	3	25.40	43.94	109.85	689.92	0.64
	4	25.40	43.94	109.85	755.31	0.70
	5	25.40	43.94	109.85	670.35	0.62
	6	25.40	43.94	109.85	729.51	0.67
	7	25.40	43.94	109.85	788.22	0.72
	8	25.40	43.94	109.85	711.27	0.65
	9	25.40	43.94	109.85	690.81	0.63
	10	25.40	43.94	109.85	640.10	0.59
Large tensile specimens	1	25.40	304.80	762.00	1842.89	0.24
	2	25.40	304.80	762.00	1988.80	0.26
	3	25.40	304.80	762.00	1939.86	0.25
Compression	1	25.40	43.94	109.85	224.15	0.92
	2	25.40	43.94	109.85	202.50	0.83
	3	25.40	43.94	109.85	229.20	0.94

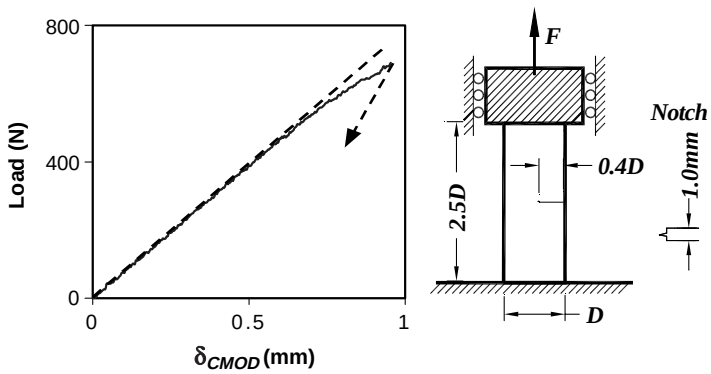

Fig. 3. A typical load–δ_{CMOD} curve in the tensile fracture test.

a Weibull-type size effect (Weibull, 1939, 1951; Bažant and Planas, 1998; Bažant, 2002). Separation of this size effect from the deterministic energetic size effect would complicate test evaluation and cause ambiguity.

2. Since a light foam such as Divinycell 100 has a smaller strength in compression than tension, significant compressive stresses (which can cause collapse of foam cells) need to be avoided. Therefore, specimens with loads applied in compression or with a ligament that is subjected to a large bending moment, for example the three-point bend tests, wedge splitting tests or compact tension tests (which are often considered more convenient), need to be avoided. Furthermore, for the same reason, the edge-notched tension specimens adopted here should not be free to rotate at ends or else a significant bending moment could be induced in the ligament. To minimize this bending moment, the ends need to be restrained against rotation even though the redundancy of restraint complicates evaluation.

3. Type I asymptotic matching law for size effect with large cracks and redundant supports

The size effect is defined as the dependence of the nominal strength, $\sigma_N = P_{\max}/bD$, as function of the characteristic specimen size (or dimension) D (here taken as the specimen width). Thus the nominal strength is a parameter of the maximum load (load capacity) having the dimension of stress. In plastic limit analysis as well as elasticity with a strength limit, σ_N is in general independent of D, which is obvious from the fact that the mathematical formulation of these theories contains no material characteristic length. Microstructural inhomogeneities, such as the cells in a foam, as well as the finiteness of the fracture process zone (FPZ), must obviously be reflected in a finite material characteristic length, which must inevitably cause a size effect unless the structural dimensions are far larger than this length.

The size effect is best visualized in a plot of $\log \sigma_N$ versus $\log D$; see Fig. 4. Now it should be noted that if the foam behaved in a ductile manner, following the theory of plasticity with no size effect, the size effect plots in Fig. 4 would have to be horizontal. The fact they are not proves that there is a size effect, in fact a very strong size effect (strong on the scale of the experiments).

Until recently, all the size effects were attributed to the randomness of strength as explained by the Weibull statistical theory. But note that if the nominal strength obeyed Weibull theory, the plot of $\log \sigma_N$

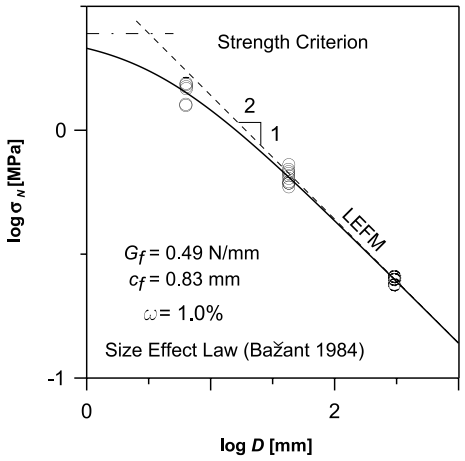

Fig. 4. Results of size effect tests of nominal strength of geometrically similar prismatic Divinycell H100 foam specimens with similar one-sided notches subjected to tension.

versus $\log D$, corresponding to the typical values of Weibull modulus, would have to be a straight line of a slope equal to $-2/m$ where m is the Weibull modulus characterizing the coefficient of variation of local material strength. Since its value is typically between 15 and 30, this straight line would have to have a slope between −0.03 and −0.07. The size effect observed (Fig. 4) is much stronger than that, overpowering any possible statistical size effect. Moreover, the use of Weibull theory is justified only if the failure is triggered by a single microscopic defect occurring randomly within a large volume, while in our case any significant defect must lie very near the tip of notch of crack (in detail, see Bažant, 2002). So the mean size effect must be deterministic (the statistical variation about the mean is another matter).

Three types of deterministic (energetic) size effect must be distinguished (Bažant, 2002). Type I is caused by relatively large notches or fatigued (stress-free) cracks formed prior to maximum load, while Type II occurs at crack initiation and is caused by a relatively large FPZ. Type III is caused by large stable crack growth in structures of initially negative geometry; it is quite similar to Type II and will not be considered here. In this section, we consider Type I.

If the tensile failure of the foam obeyed linear elastic fracture mechanics (LEFM), the logarithmic size effect plot would have to be a straight line of downward slope −1/2, shown in Fig. 4. The results are very close to that line, which means that, on the scale of the tests (and of course on larger scales), the material behaves in an almost brittle manner. The term 'brittle' is understood as the adherence to LEFM, while the term 'quasibrittle' refers to nonlinear cohesive softening (nonductile) fracture with a large FPZ, deviating from LEFM (on the other hand the term 'ductile fracture' refers to cohesive plastic, or nonsoftening, fracture behavior, in which most of the nonlinear zone surrounding the crack tip is plastically yielding and the softening FPZ is still very small).

According to the size effect method of measuring nonlinear fracture properties (Bažant and Pfeiffer, 1987; Bažant and Kazemi, 1990; Bažant and Planas, 1998), the location in Fig. 4 of the asymptote of slope −1/2 determines the fracture energy G_f of the material, and the rate at which this asymptote is approached determines the effective size of the FPZ, c_f, representing the distance from the actual crack tip to the tip of an equivalent LEFM crack, which lies roughly in the middle of the FPZ and can be precisely defined as the tip location that gives the best LEFM fit of the actual size effect curve. Based on G_f and c_f, one can also determine the fracture toughness and the critical crack-tip opening displacement:

$$K_c = \sqrt{E'G_f}, \quad \delta_{CTOD} = \sqrt{8G_f c_f/E'}/\pi \tag{1}$$

where for plane stress $E' = E =$ Young's modulus, and for plane strain $E' = E/(1-\nu^2)$, $\nu =$ Poisson's ratio; δ_{CTOD} is a material length parameter introduced for fracture of metals by Cottrell (1963) and Wells (1961).

Although the most general derivation of the size effect method can be given on the basis of asymptotic expansion of the J-integral, let us sketch the brief and simple derivation from equivalent LEFM presented in Bažant and Planas (1998) and extended in Bažant and Kazemi (1990) (see also Bažant and Planas, 1998; Bažant, 2002). The use of equivalent LEFM has the advantage of providing an approximate dependence of the size effect law parameters on the geometry. The energy release rate in LEFM may always be expressed as

$$\mathscr{G} = K_I^2/E' = \sigma_N^2 g(\alpha) D/E' \tag{2}$$

where $\alpha = a/D =$ relative crack length, $a =$ actual crack length, $g(\alpha) = [k(\alpha)]^2 =$ dimensionless energy release function of relative crack length α, $k(\alpha) = K_I/\sigma_N D =$ dimensionless stress intensity factor, and $K_I =$ actual stress intensity factor (we consider only mode I). In the present case, the fracture geometry is positive (i.e., the derivative $g'(\alpha) > 0$), and in that case the FPZ at maximum load must still be attached to the notch tip and the crack begins to propagate at decreasing load. So the maximum load occurs as soon as the crack propagation condition $\mathscr{G} = G_f$ is attained. This yields for the nominal strength $\sigma_{N_u} = \sigma_N$ at maximum load the well-known general LEFM expression:

$$\sigma_{N_u} = \sqrt{E' G_f / g(\alpha) D} \tag{3}$$

Since the FPZ at maximum load is still attached to the notch tip, we may use the approximation $a = a_0 + c_f$ or

$$\alpha = \alpha_0 + \theta \quad \text{with} \quad \alpha_0 = a_0/D, \quad \theta = c_f/D \tag{4}$$

where a_0 is the length of notch or preexisting traction-free crack; c_f = material constant $\approx$ half-length of the FPZ (Bažant and Kazemi, 1990; Bažant and Planas, 1998).

The size effect for geometrically similar specimens (i.e., specimens for which α_0 = constant) could be simply described by substituting $\alpha = \alpha_0 + \theta$ into (3). However, such an approximation would be valid only for large sizes D because for small enough D the argument of $g(\alpha)$ becomes larger than the range of α for which $g(\alpha)$ is defined. To find a size effect law applicable for all sizes, we write an asymptotic expansion in terms of $1/D$;

$$g(\alpha) = g(\alpha_0 + c_f/D) = g(\alpha_0) + g'(\alpha_0) c_f/D + (\cdots)/D^2 + \cdots \tag{5}$$

Truncating it after the second term, we get from (3) the size effect law proposed by Bažant (1984) and Bažant and Kazemi (1990):

$$\sigma_{N_u} = \sqrt{\frac{E' G_f}{[g(\alpha_0) + g'(\alpha_0) c_f/D] D}} = \frac{\sigma_{N_0}}{\sqrt{1 + D/D_0}} \tag{6}$$

in which,

$$\sigma_{N_0} = \sqrt{\frac{E G_f}{g'(\alpha_0) c_f}}, \quad D_0 = c_f \frac{g'(\alpha_0)}{g(\alpha_0)} \tag{7}$$

D_0 represents the transitional size delineating the brittle behavior from nonbrittle (ductile) behavior and corresponds to the intersection of the asymptotes in Fig. 4; D_0 and σ_{N_0} are constant because, owing to geometric similarity, α_0 is a constant for all the specimens tested. The ratio $\beta = D/D_0$ is called the brittleness number (Bažant and Planas, 1998); $\beta \gg 1$ means a very brittle response, close to LEFM, and $\beta \ll 1$ means a very ductile response. To be able to identify the material fracture parameters from size effect tests, the range of β must be sufficiently broad (in this regard, note that variation of the ratio $g'(\alpha)/g(\alpha)$ due to changes in geometry, e.g., the relative notch depth, helps to increase the range of β).

The truncation of (5) after the second asymptotic term has been lucky since it happens to yield a law approximately applicable through the entire size range. The reason is that, by chance, it happens to produce a so-called 'asymptotic matching' formula—a smooth formula that has the correct asymptotic properties at all extremes, i.e., not only for $D \to \infty$ but also for $D \to 0$. It can be shown (most rigorously on the basis of the cohesive crack model) that the limit of σ_N for $D \to 0$ must be a positive constant, σ_{N_0}, and that this constant must be approached linearly, i.e.,

$$\sigma_N \approx \sigma_{N_0} - \kappa_1 D \quad \text{for} \quad D \to 0 \tag{8}$$

where κ_1 is a positive constant. By luck, the law (6) is the simplest formula satisfying this small-size asymptotic condition. However, if more than two terms of the large size asymptotic expansion were retained, the small-size asymptotic condition would be violated (therefore, a different approach must be taken if a more accurate size effect law is desired; Bažant, 2002, Section 9.7).

Because the end supports of the specimen are redundant (i.e., statically indeterminate), function $g(\alpha)$ cannot be taken directly from handbooks. This aspect was handled for kink bands in fiber composites in a simplified way (Bažant et al., 1999). Here a new approach that is exact within the framework of equivalent LEFM will be formulated.

Due to the redundancy provided by the rotational restraints at the ends, the axial load resultant $P_{\max}$ shifts when the specimen size is increased. In other words, the eccentricity e of the maximum axial load with respect to mid-thickness must be a function of α. To calculate the function $e(\alpha)$, we use the condition of a vanishing relative rotation between the specimen ends:

$$\Delta\phi = PeC_{MM} + PC_{PM} = 0 \tag{9}$$

where Pe is the bending moment; C_{MM}, C_{PM} are the compliances of the cracked specimen which can be calculated from the α-dependence of the dimensionless stress intensity factors $k_M(\alpha) = K_{MM}bD^{3/2}/M$ and $k_P(\alpha) = K_{PP}b\sqrt{D}/P$, where K_{MM} and K_{PP} are the actual mode I stress intensity factors due to unit bending moment M and to unit axial force P applied at mid-thickness (i.e., at $\alpha = 1/2$), respectively. Based on the energy relations of LEFM (Eq. (3.5.18) in Bažant and Planas, 1998),

$$C_{PM}(\alpha) = \frac{12}{bE'D}\int_0^\alpha k_P(\alpha')k_M(\alpha')\,\mathrm{d}\alpha', \quad C_{MM}(\alpha) = \frac{12L}{bE'D^3} + \frac{72}{bE'D^2}\int_0^\alpha [k_M(\alpha')]^2\mathrm{d}\alpha' \tag{10}$$

where the term $12L/bE'D^3$ L represents the bending compliance of a specimen with no crack and no notch (L = specimen length), and the integrals represent the additional compliances due to the notch and the crack. According to the well-known expressions for the stress intensity factors for the present specimen geometry (Tada et al., 1985),

$$k_P(\alpha) = \sqrt{\pi\alpha}(1.122 - 0.231\alpha + 10.55\alpha^2 - 21.71\alpha^3 + 30.38\alpha^4) \tag{11}$$

$$k_M(\alpha) = \sqrt{\pi\alpha}(1.122 - 1.40\alpha + 7.33\alpha^2 - 13.08\alpha^3 + 14.0\alpha^4) \tag{12}$$

According to the principle of superposition, the dimensionless stress intensity factor and the energy release rate caused by a combination of bending moment Pe and centric axial force P is

$$k(\alpha) = k_P(\alpha) + 6(e/D)k_M(\alpha), \quad g(\alpha) = [k(\alpha)]^2 \tag{13}$$

Solving e from (9), we thus get

$$g(\alpha) = \left(k_P(\alpha) - \frac{6C_{PM}(\alpha)}{C_{MM}(\alpha)D}k_M(\alpha)\right)^2 \tag{14}$$

4. Analysis of Type I size effect test results for tensioned specimens

The known functions $k_P(\alpha)$ and $k_M(\alpha)$ can now be used to calculate the energy release function and its derivative; $g(\alpha_0) = 2.19$, $g'(\alpha_0) = 8.43$ where $\alpha_0 = 0.4$ (Section 2). Then one may use the size effect law equations (6) and (7) to identify G_f and c_f by means of optimum fitting of the data points in Fig. 4. These equations can be easily fitted to the test data by either nonlinear optimization (using, e.g., the Levenberg–Marquardt algorithm) or linear regression. The latter is made possible by rearranging Eq. (6) to an expression for σ_N^{-2} as a function of D, which represents a linear regression plot (Fig. 5). The optimum fit, in the least-square sense, is shown by the curve in Fig. 4. From the optimum values of $D_0 = 3.18$ mm and $\sigma_{N_0} = 2.48$ MPa, and knowing $G_f = \sigma_{N_0}^2 D_0 k(\alpha_0)^2/E'$, $c_f = k(\alpha_0)D_0/2k'(\alpha_0)$, one can identify G_f, c_f and from these values then the other fracture properties. The results for the present foam are

$$G_f = 0.49\ \mathrm{N/mm}, \quad c_f = 0.83\ \mathrm{mm}, \quad K_c = 6.53\ \mathrm{N/mm^{3/2}}, \quad \delta_{\mathrm{CTOD}} = 0.10\ \mathrm{mm} \tag{15}$$

The values of G_f and f_t' together characterize the initial slope of the softening curve of the cohesive model (Guinea et al., 1997), which is all that is needed to calculate the maximum loads of structures. Knowledge of

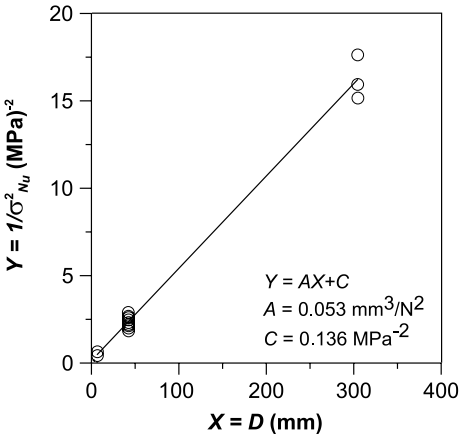

Fig. 5. Linear regression based on asymptotic matching formula (6).

these material parameters makes it possible to analyze the size effect due to fracture in the core of a sandwich plate by equivalent LEFM, or cohesive crack model, or crack band model.

The size effect law (6) applies only if either a large notch or a large fatigued (stress free) crack (or damage zone) develops before the maximum load. When there is neither a large notch nor a preexisting large crack (or damage zone) with a reduced stress, the response of the foam tends to be ductile and, at larger strain, locking (Gibson and Ashby, 1997). This is a major difference from quasibrittle material such as concrete, in which a large tensile cracking zone develops and causes stress redistribution which again leads to size effect. This size effect is of a very different type and, unlike the size effect associated with large cracks, approaches the Weibull statistical size effect at very large sizes (Bažant, 2002).

5. Size effect tests of V-notched specimens in compression

Compressive tests of V-notched specimens of Divinycel H100 foam have been also conducted to clarify the nature of cell collapse. The test results were found to exhibit no size effect. This means that the stress concentration at the tip of the V-shaped notch could not have caused any strain-softening response. Rather, the cells of the foam must have collapsed plastically, with no stress reduction. Therefore, the usual plasticity type analysis is justified for the compressive failure of vinyl foam (this conclusion, though, is probably not true for foams made from very brittle materials).

Furthermore, it was observed that when the notch angle is not wide enough, the opposite faces of the V-notch come into contact and produce a locking behavior in which the compressive stress magnitude increases. This is the same behavior as seen in compression specimens with no notches nor preexisting cracks (Gibson and Ashby, 1997). Empirically, the minimum angle to prevent closing of the notch near its tip is about 90° (Fig. 6).

6. Analysis of Type I three-point-bend size effect data of Zenkert and Bäcklund (1989)

These size effect test data were also fitted by Eq. (6), as shown in Fig. 7. The cellular material that they used was a slightly heavier closed-cell vinyl foam with cell size about 0.3 mm (Divinycell H200, supplied by Diab-Barracuda AB in Laholm, Sweden). These tests used three-point bend beams with the same thickness

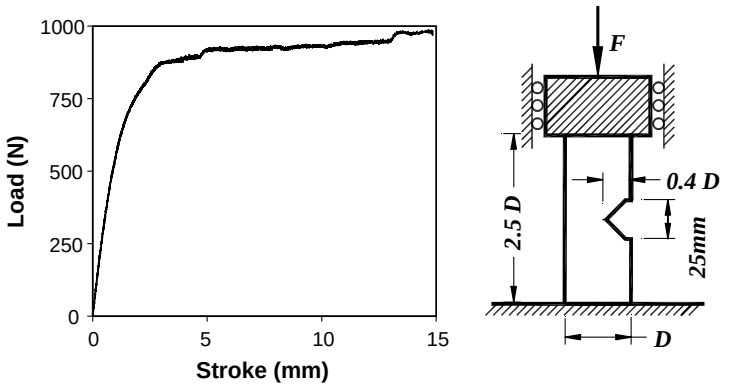

Fig. 6. Test specimens for compression and load–deflection curve demonstrating lack of softening (which implies the absence of size effect in compression).

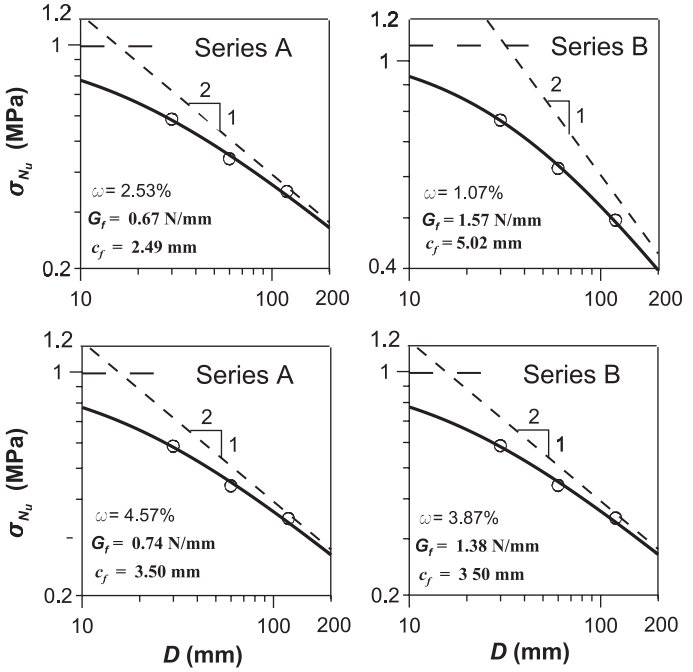

Fig. 7. Fit of Zenkert and Bäcklund's (1989) for three-point bend beams by Bažant's size effect law (1984) (solid line). Dashed line: LEFM. Dash-dot line: strength criterion. Series A (left) and B (right) pertain to different temperature conditions and material from different blocks. Top: Fits when both G_f and c_f are optimized separately for each series. Bottom: Fits when c_f is forced to be the same for both series while G_f values are allowed to be different.

$b = 30$ mm, the same span/depth ratio, $L/D = 4$, and the same ratio of notch length to specimen depth, $\alpha = 0.5$, but different beam depths $D = 30$, 60 and 120 mm.

Two series of size effect tests, labeled A and B, were performed by using specimens cut from two different blocks of the foam and subjected to slightly different temperature conditions. There were appreciable differences between these two series, which must be due to differences in temperature conditions as well as

notoriously high randomness of foam properties and perhaps uncontrollable differences in specimen manufacture. The randomness is documented by very high scatter of the fracture toughness values, K_{I_c}, measured by Zenkert and Bäcklund on specimens cut from different blocks of material. After measuring the peak loads, they calculated the toughness according to LEFM as $K_{I_c} = \sigma_{\infty c}\sqrt{\pi a} f(a/D)$, with $f(a/D)$, given by a handbook, and reported $G_{I_c} = K_{I_c}^2/E' = 0.50, 0.59, 0.71$ N/mm for $D = 30, 60, 120$ mm in test series A, and 0.84, 1.09, 1.38 N/mm in test series B, respectively (note that the ASTM requirement for LEFM validity, namely that each of the crack, ligament and cross section dimension must be longer than $2.5(K_{I_c}/\sigma_y)^2$, was not fully satisfied).

The specimens of series A had generally much lower maximum loads than the counterpart specimens of series B. The values of G_f and c_f for Zenkert and Bäcklund's data can now be again easily calculated by optimum fitting of the size effect law (6) with (7) to the nominal strength data. The results are:

$$G_f = 0.74 \text{ N/mm}, \quad c_f = 3.5 \text{ mm} \quad \text{for series A} \tag{16}$$

$$G_f = 1.38 \text{ N/mm}, \quad c_f = 3.5 \text{ mm} \quad \text{for series B} \tag{17}$$

when the fits are optimized forcing the c_f value to be the same for both series (Fig. 7 bottom). If both c_f and G_f are allowed to be different for each series, the optimum fits are only slightly better (see Fig. 7 top). On the other hand, if both c_f and G_f are forced to be the same for both series, the optimum fits get much worse.

7. Type II asymptotic matching law for size effect at crack initiation in holed panels

Specimens of a different type—flat panels with central holes instead of notches—were used in fracture tests of Fleck et al. (2001) and Olurin et al. (2001); see Fig. 8. The holed specimens fail at the initiation of macroscopic (continuous) crack from the hole. A finite FPZ, of a size denoted as $2c_f$, must form before a crack can propagate. Therefore the equivalent LEFM crack at the initiation of propagation has approximately the length c_f.

The problem is mathematically similar to the initiation of a compression kink band from a hole in a fiber composite panel, which was analyzed in Bažant et al. (1999) (the main difference was that, in contrast to the tensile cohesive stress in crack, the kinking of axial fibers causes the axial compressive stress to drop to a certain finite residual value rather than to zero). Here we present a more general analysis of asymptotic matching type.

We start again from the general relation (3) in which $g(\alpha)$ is now replaced by the dimensionless energy release function $g(\alpha, \rho)$ with two arguments, $\alpha = 2a/D$ and $\rho = 2R/D$; $D =$ panel width, $R =$ radius of the hole; and the crack length a is measured from the center of the hole; see Fig. 8. When $c = a - R \ll R$, the stress intensity factor K_I must obviously be nearly the same as that for a normal surface crack of depth c in an elastic half-plane, which is $K_I = 1.12\sigma\sqrt{\pi c}$. This implies that $g(\alpha, \rho) \approx 1.12^2\pi(a - R)/D$ when $c \ll R$.

One might think that the size effect would be captured simply by substituting

$$\alpha = \alpha_0 + \theta \quad \text{with} \quad \alpha_0 = 2R/D, \quad \theta = 2(a - R)/D \tag{18}$$

However, like for Type I, the resulting size effect formula would be applicable only for very large sizes because α exceeds its physical range for small enough D. Now we must realize that, since the equivalent LEFM is realistic only asymptotically for large enough D, function $g(\alpha, \rho)$ may be replaced by some other more convenient function with the same large-size asymptotic properties. To find the convenient function, we begin, similar to (5), with the asymptotic expansion in terms of $1/D$:

$$g(\alpha, \rho) = g'(\alpha_0, \rho)\frac{2c_f}{D} + \frac{g''(\alpha_0, \rho)}{2!}\frac{4c_f^2}{D^2} + \cdots \tag{19}$$

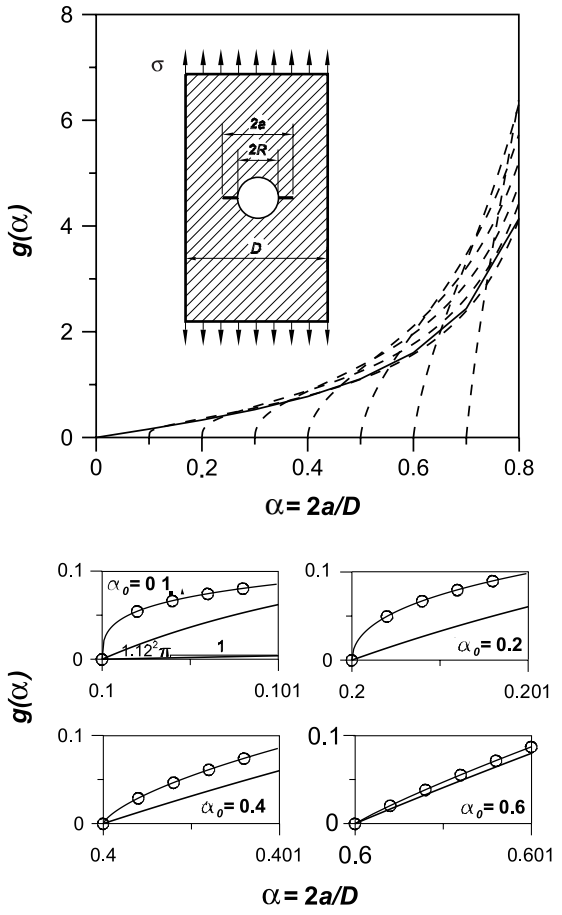

Fig. 8. Top: Dimensionless energy release function $g(\alpha)$ for isotropic specimens with centric holes of different radii (the solid curve represents function $g(\alpha)$ for a specimen with a centric horizontal crack of length $2a$). Bottom: Corrected energy release function with a finite slope at crack initiation from the hole (heavy lines), compared to Führing's solution (thin lines).

Here we omitted the first term because $g(\alpha_0, \rho) = 0$ (due to the absence of any notch or preexisting traction-free macroscopic crack). For this reason, we cannot truncate the expansion after the linear term, like we did for Type I. So we truncate it after the quadratic term and substitute it into (3). Thus we obtain

$$\sigma_{N_u} = \sqrt{\frac{E' G_f}{2 c_f g'(\alpha_0, \rho)(1 - 2\xi)}} \tag{20}$$

with

$$\xi = \frac{c_0}{D}, \quad c_0 = c_f \frac{(-g''(\alpha_0, \rho))}{2g'(\alpha_0, \rho)} \tag{21}$$

Here we include the minus sign in the definition of ξ because, in all the cases where the size effect occurs, $g''(\alpha_0, \rho) < 0$ (while $g'(\alpha_0, \rho) > 0$) where the primes denote partial derivatives with respect to α. These are the cases in which the profile of tensile stress acting before fracture decreases in the direction away from the

surface (if it increases, then $g'' > 0$, in which case the crack grows stably and the maximum load does not occur at crack initiation but later).

Unfortunately, unlike Type I, Eq. (20) cannot describe the size effect through the full range of $D \in (0, \infty)$ because, for small enough D, $1 - 2\xi$ becomes negative and σ_N imaginary. To recover from this snag, we must realize that only the first two large-size asymptotic terms of (20) are realistic. Any convenient function that shares these two terms is equally good asymptotically for $D \to \infty$. Aware of this point, we try the following asymptotic approximations verified by Taylor series expansions in terms of $\xi = c_0/D$:

$$(1 - 2\xi)^{-1/2} \approx 1 + \xi \approx (1 + r\xi)^{1/r} \quad (\text{for } \xi \ll 1) \tag{22}$$

where r can be an arbitrary positive empirical parameter. From (20) we thus obtain:

$$\sigma_{N_u} = \sqrt{\frac{E' G_f}{2 c_f g'(\alpha_0, \rho)}} q(D), \quad q(D) = (1 + r\xi)^{1/r} \tag{23}$$

This formula along with (21), which is second-order accurate in $1/D$ for $D \to \infty$, has the general form of the size effect law for failure at crack initiation, derived for concrete in Bažant and Li (1996) and extended by the addition of empirical parameter r in Bažant (1998) (see also Bažant and Planas, 1998; and Bažant, 2002). Eq. (23) with (21) is also analogous to the formula derived in Bažant et al. (1999, Eq. (54)) for the propagation of compression kink bands with a finite residual stress in orthotropic fiber composites.

Eq. (23) overcomes the problem with imaginary σ_N for small enough D. However, the asymptotic behavior for $D \to 0$ is still not entirely satisfactory because $\sigma_N \to \infty$. This asymptotic behavior (shared by the famous Hall–Petch formula for the effect of crystal size on the yield strength of a polycrystalline metal) might seem acceptable because specimen size D less than the inhomogeneity size (cell size in foam) is impossible. However, from the viewpoint of the cohesive crack model, such small-size asymptotic behavior is not right. Yet it can be remedied easily. We simply replace D with (D + constant) in the definition of ξ, which means that expression (21) for ξ, to be used for function $q(D)$ in (23), is now replaced by

$$\xi = \frac{c_0}{D}, \quad c_0 = \frac{(-g''(\alpha_0, \rho))}{2g'(\alpha_0, \rho)} \frac{c_f}{\eta c_f + D} \tag{24}$$

where η is a dimensionless empirical positive constant, which will be here taken as $\eta = 1$ for lack of sufficiently extensive test data. Obviously, (24) will make the small-size asymptotic properties conform to (8). At the same time, the first two terms of the large-size asymptotic approximation will remain unchanged. This may be verified by the following asymptotic approximations, second-order accurate in $x = c_f/D$:

$$\begin{aligned} \sigma_{N_u} \propto (1 + r\xi)^{1/r} &= \left(1 + \frac{s r c_f}{\eta c_f + D}\right)^{1/r} = \left(1 + \frac{srx}{1 + \eta x}\right)^{1/r} = \left(\frac{1 + (\eta + sr)x}{1 + \eta x}\right)^{1/r} \\ &\approx \frac{1 + (s + \eta/r)x}{1 + (\eta/r)x} \approx \left[1 + \left(s + \frac{\eta}{r}\right)x\right]\left(1 - \frac{\eta}{r}x\right) \approx 1 + sx = 1 + \frac{s c_f}{D} \end{aligned} \tag{25}$$

where s is a positive constant.

8. Analysis of test data for holed panels

Olurin et al. (2001) and Fleck et al. (2001) conducted a rather extensive series of tensile fracture tests on Divinycell panels of width D in the range (10 mm, 100 mm), and $2R/D$ in the range of (0, 0.6), with the length $L = 1.5D$ and the thickness $b = 10$ mm. The geometry of the test is shown in Fig. 8 and the measured data are the points in Fig. 9 showing the dependence of the nominal strength σ_{N_u} and of the net average

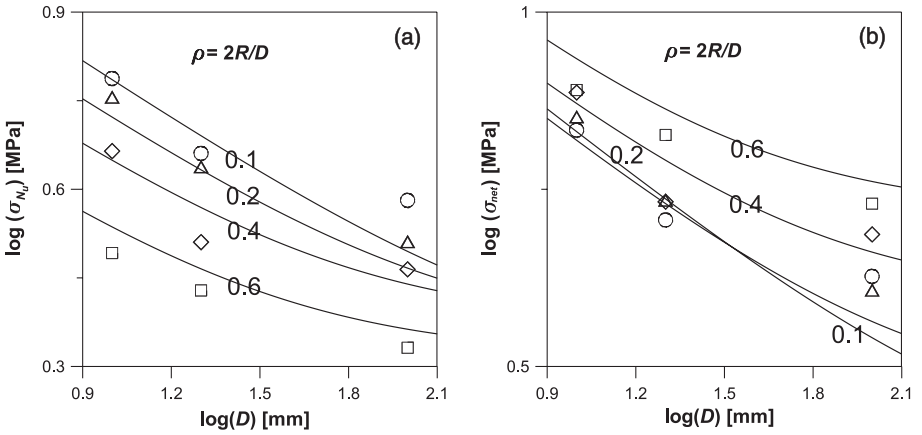

Fig. 9. Fleck et al.'s (2001) test data for holed panels, plotted (a) in terms of the average tensile stress σ_{N_u} applied at ends, and (b) in terms of the average net cross section stress (the solid curves show the fits by the present theory).

strength $\sigma_{\text{net}} = \sigma_{N_u} D/(D-2R)$ on the specimens size D and relative hole size $\rho = R/2D$, where σ_{N_u} is the average tensile stress applied at the specimen ends (Fig. 8). Let us try to exploit these data for checking the present theory. In principle, it must be possible to describe these data by (21) with (24). The function $g(\alpha)$ may be expected to be approximately the same as that for an infinite strip with a hole, for which it is presented in handbooks (Tada et al., 1985; Murakami, 1986; see Fig. 8). The available function, however, is found to have incorrect asymptotic properties for $\alpha \to \alpha_0$, yet these properties are crucial for the present asymptotic approach. Instead of $g(\alpha)$, the handbooks give for $K_{\text{I}}(\alpha)$ formulae that satisfy the obvious asymptotic conditions $\lim(\mathrm{d}K_{\text{I}}/\mathrm{d}\alpha) = \infty$ for $\alpha \to \alpha_0$ as well as $\lim K_{\text{I}} = 0$ (which implies that $\lim g(\alpha) = \lim K_{\text{I}}^2/E' = 0$). However, it is also necessary that

$$0 < \lim_{\alpha\to\alpha_0} g'(\alpha) < \infty, \quad \lim_{R/D\to 0}[\lim_{\alpha\to\alpha_0} g'(\alpha)] = 1.12^2\pi, \quad -\infty < \lim_{\alpha\to\alpha_0} g''(\alpha) < 0 \tag{26}$$

These conditions may be easily proven by noting that the scale transformation of coordinates centered at the crack mouth making the ratio $a/(a-R)$ arbitrarily small produces the same situation as a crack initiating from a planar surface and, when both $R/D \to 0$ and $a/(a-R) \to 0$, the same situation as a crack initiating from the surface of an elastic halfspace. For that situation, $K_{\text{I}} = 1.12\ \sigma_N\sqrt{\pi c}$ with $c = a - a_0 =$ crack length, which implies that $g(\alpha) = K_{\text{I}}^2/\sigma^2 D = 1.12^2\pi c/D$ and $g'(\alpha) = 1.12^2\pi < \infty$. The handbook expressions violate this condition, reflected in (26), giving incorrectly $\lim g'(\alpha) \propto \lim K_{\text{I}}^2 = \infty$ (see Fig. 8 where the correct initial slopes of each curve for small enough R/D are marked). They also incorrectly give $\lim g'' = -\infty$. These discrepancies are no big problem for most engineering applications but are a fatal fault for the present analysis based on asymptotic matching.

It may nevertheless be assumed that the handbook formulae are good enough for not too short cracks. So, it has been tried to devise a correction that would satisfy conditions (26) and fit the existing formula very closely except in the initial portion $\alpha - \alpha_0 < 0.05$ of each curve. After some trials, the following smooth formula has been adopted for this purpose

$$g(\alpha) = (1-\alpha)^{-1}\sum_{n=1}^{5} b_n(\alpha-\alpha_0)^n + b_6\{1-[1+b_7(\alpha-\alpha_0)]^{-3}\} \tag{27}$$

(see Fig. 8) and has been optimally fitted (using the Levenberg–Marquardt optimization algorithm) to the curve of Führing's (1973) formula given by Murakami (1986) for each fixed R/D, ignoring the points for

Table 2
Parameters controlling the curve match of $g(\alpha)$

	$\alpha_0 = 0.1$	$\alpha_0 = 0.2$	$\alpha_0 = 0.4$	$\alpha_0 = 0.6$
a	2.13	3.24	7.42	16.71
b	−5.09	−10.68	−36.74	−124.78
c	10.52	27.04	126.57	682.72
d	−11.19	−35.02	−234.68	−2248.45
e	5.22	18.49	175.54	3111.67
f	0.14	0.24	0.34	0.28
g	197.09	93.71	52.59	49.64
$g'(\alpha_0)$	86.92	71.52	65.22	83.77
$g''(\alpha_0)$	−66 663	−25 307	−11 200	−8754

$g(\alpha) < g_0/2$ where $g_0 =$ value of $g(\alpha)$ for α equal to the actual α_0 but $R = 0$ (for the values of b_n for various $\rho = 2R/D$, see Table 2). This new dimensionless energy release function (27) satisfies the asymptotic inequalities (26), although the limiting values $g'(\alpha_0)$ and $g''(\alpha_0)$ are doubtless still in error.

With the first and second derivatives at α_0 for each R/D ensuing from (27), the fit of all the data of Fleck et al. (2001) for various D and R has been simultaneously optimized with the Levenberg–Marqardt algorithm; see the curves and the data points plotted in various coordinates in Figs. 9 and 10. The plots in Fig. 10a–c are based on rearranging (21) with (24) as follows:

$$\sigma_{N_u}\sqrt{2g'} = \sqrt{\frac{E'G_f}{c_f}}\left[1 + \frac{(-g'')}{2g'}\,\frac{rc_f}{D}\right]^{1/r} \tag{28}$$

or

$$Y = AX + C \tag{29}$$

where

$$X = r(-g'')/2g'D, \quad Y = (\sigma_{N_u}\sqrt{2g'})^r, \quad A = c_f C, \quad C = (E'G_f/c_f)^{r/2} \tag{30}$$

in which we use the abbreviated notations $g' = g'(\alpha_0, \rho)$, $g'' = g''(\alpha_0, \rho)$. Another instructive linear plot is obtained by further rearranging (29) as follows:

$$Y' = A'X' + C' \tag{31}$$

where

$$X' = Y, \quad Y' = c_f^{1-r/2}X, \quad A' = (E'G_f)^{-r/2}, \quad C' = -c_f^{-r/2} \tag{32}$$

The plots in Fig. 10a–c use coordinates for which the data for all $\rho = 2R/D$ should ideally lie on one and the same curve. The curved plot in Fig. 10a is based on (28) and has the statistical advantage that the data points are less crowded together than in the other plots. The plots in Fig. 10b and c are linear, representing linear regressions based on (29) and (31).

The linear plot in Fig. 10b, based on (29), can be used to obtain the optimum material parameters from a sequence of linear regressions. One needs to choose a series of r values, and for each r the linear regression of the data then yields A and C as well as their statistics. From A and C one can calculate $c_f = A/C$, and then $E'G_f = C^{2/r}/c_f$.

In linear regression, the slope A or A' is generally obtained with a greater accuracy than the intercept C or C'. Since (for a fixed r and E') the slope A' depends only on G_f, the linear plot in Fig. 10c, therefore, directly reveals the statistical scatter of $G_f^{r/2}$ (whose coefficient of variation is about $r/2$ times the coefficient of variation of G_f).

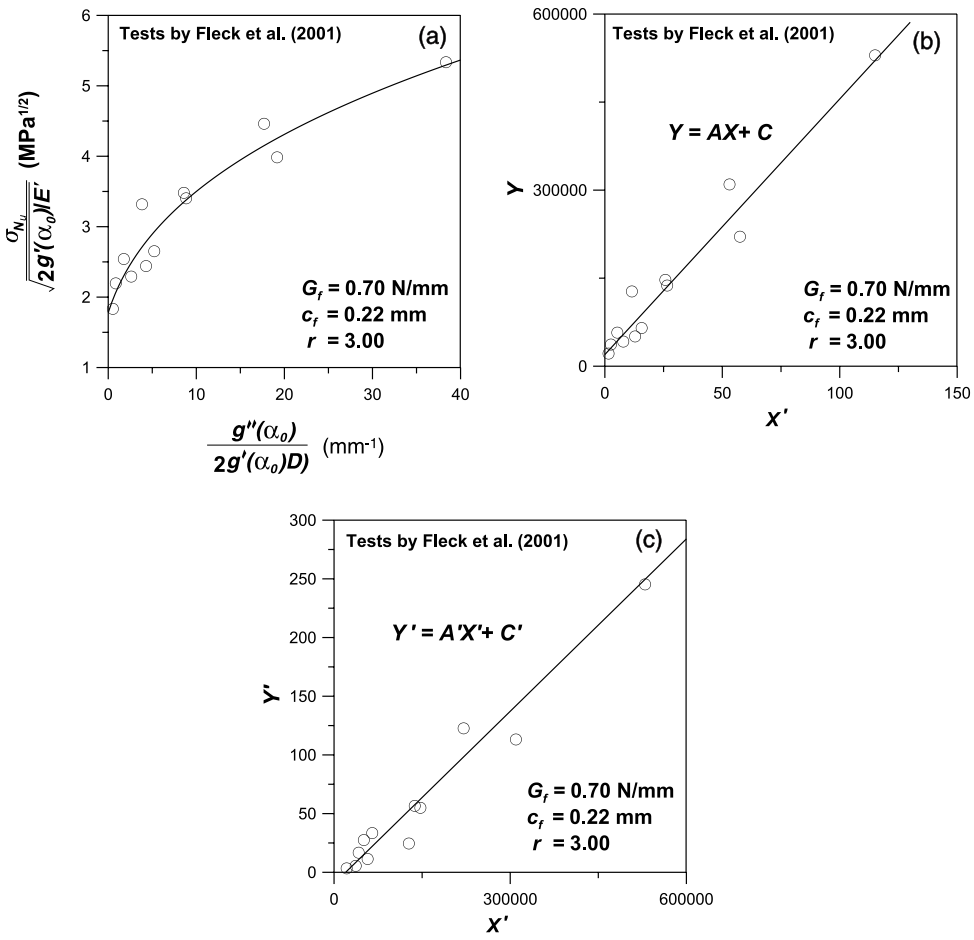

Fig. 10. Optimum fits of Fleck et al.'s (2001) test data for holed panels: (a) by Eq. (28), (b) by Eq. (29), (c) by Eq. (31).

The values of G_f, c_f and r corresponding to the optimum fits are shown in each figure. In this case, however, these values should not be regarded as good estimates of the material properties, because (a) unnotched specimen failing at crack initiation are generally much less suitable for determining fracture energy than notched specimens because the results are much less sensitive to the value of G_f; and, (b) because, more seriously, the present optimum fits have been obtained with rather inaccurate estimates of $g'(\alpha,\rho)$ and $g''(\alpha,\rho)$.

Therefore, the present analysis of Fleck et al.'s (2001) data merely proves that a formula derived from fracture mechanics can describe the nominal strength of prismatic specimens of different sizes with holes of different sizes. It is not proven that accurate predictions would be impossible if G_f and c_f were determined by other means (from notched tests). Examining this point would require solving function $g(\alpha,\rho)$ with correct asymptotic properties.

For the range of Fleck et al.'s (2001) data, the values of $\theta = (a - a_0)/R$ do not go out of the range $(\alpha_0, 1)$, and so it is actually possible to also fit the data directly with the original formula (3) in which $\alpha = \alpha_0 + c_f$. The fits of the data in Fig. 10 with formula (3), obtained easily with a nonlinear optimization algorithm, are slightly worse than those shown in Figs. 9 and 10 and the optimum values of G_f and c_f are rather different

(though not different in terms of the order of magnitude). Doubtless the reason is that (3) is not an asymptotic matching formula, i.e., a formula with a realistic asymptotic behavior for very small sizes.

The smallest holes in Fleck et al.'s (2001) specimens have a radius R of the same size as the size of the FPZ. In that case, in principle, G_f and c_f could depend on R. To check it, it was assumed that $G_f = G_1 + G_2 R^n$ and $c_f = c_1 + c_2 R^n$ (in which G_1, G_2, c_1, c_2 and n are constants), and the data were fitted again. However, the optimum fits achievable did not become any better. It follows that the effect of curvature of the surface bordering the FPZ is not significant.

It must be admitted that a certain error in the present analysis arises from taking function $g(\alpha, \rho)$ the same as for an isotropic material. In reality, a Divinycell foam exhibits a slight orthotropy due to the gravity effect during casting (which was considered in Brocca et al. (2001), based on the generalization of LEFM by Bao et al., 1992). Although the consideration of orthotropy would probably alter this function somewhat, the difference appears to be insignificant compared to the inevitable scatter of test data.

9. Verification by simulation of tensile fracture test with cohesive crack model

Hillerborg et al. (1976), Hillerborg (1985) and Petersson (1981) analyzed mode I cohesive fracture by condensing out from the structural stiffness matrix all the nodes other than those on the crack line and at the load point. In their approach, one begins by calculating the compliance matrix for the crack surface nodes and the load point (see also Bažant and Planas, 1998). The governing equation is then obtained from the crack compatibility condition which, in dimensionless form (Zi and Bažant, 2003), reads:

$$\bar{w}(\xi) = -\bar{D}\int_{\alpha_0}^{\alpha} \bar{C}(\xi, \xi')\bar{\sigma}(\xi')\,\mathrm{d}\xi' + \bar{D}\bar{\sigma}_N \bar{C}^N(\xi) \tag{33}$$

which must be coupled with the condition that the stress intensity factor at the cohesive crack tip $K_I = 0$; here $\xi = x/D =$ dimensionless coordinate, $\bar{D} = \sigma_f D/Ew_f = D/2l_{ch}$ dimensionless size ($l_{ch} = EG_f/f_t'^2 =$ Irwin's (1958) characteristic length), $\bar{w} = w/w_c =$ dimensionless crack opening displacement, $w_c =$ critical opening displacement at which cohesive stress attains zero, $\bar{\sigma} = \sigma/f_t' =$ dimensionless shear stress, $f_t' =$ material strength, $\alpha_0 = a_0/D =$ dimensionless length of notch, $\bar{C}^N = C^N E/D =$ dimensionless compliance corresponding to the nominal stress $\bar{\sigma}_N = \sigma_N/f_t'$, $\bar{C} = EbC =$ compliance for the stress in FPZ, i.e., $\bar{w}$ at ξ caused by unit stress $\bar{\sigma}$ at ξ' (C^N and $C =$ actual compliances).

In Hillerborg and Petersson's approach, the load and load–point displacement are solved from the crack compatibility condition of the type of (33) (coupled with the condition $K_I = 0$) for cohesive crack tip placed in a crack line node, one after another. This means that the entire history of displacement distributions for increasing loads must be followed for each specimen size even though only the peak load is needed for size effect studies.

Li and Liang (1993) and Li and Bažant (1994) (in a discrete form), and Bažant and Li (1995) (in a continuous form), developed a procedure that is much more efficient for size effect studies (see also Bažant and Planas, 1998, Sec. 7.5.4) because it does not necessitate integrating the deformation history, allowing the peak load to be calculated directly. Recently, this procedure, used initially for positive geometries, was generalized for negative-positive geometries for which the energy release rate first decreases with crack advance and later increases (Zi and Bažant, 2003). In this approach, the problem of directly calculating σ_N for various D is recast as an eigenvalue problem. The size D for which a given α corresponds to the peak load is the eigenvalue of the following dimensionless homogeneous Fredholm integral equation (Bažant and Li, 1995):

$$\bar{w}_{,\alpha}(\xi) + \bar{D}\int_{\alpha_0}^{\alpha} \bar{C}(\xi, \xi')\bar{\sigma}_{,\bar{w}}\bar{w}_{,\alpha}(\xi')\,\mathrm{d}\xi' = 0 \tag{34}$$

This equation is linear when the softening stress–displacement law of the cohesive cracks is linear (i.e., when $\bar{\sigma}_{,\bar{w}}$ is constant). The dimensionless nominal strength is then obtained by

$$\bar{\sigma}_{N_u} = \frac{\int_{\alpha_0}^{\alpha} \bar{w}_{,\alpha}(\xi)\,\mathrm{d}\xi}{\bar{D}\int_{\alpha_0}^{\alpha} \bar{C}^N(\xi)\bar{w}_{,\alpha}(\xi)\,\mathrm{d}\xi} \tag{35}$$

Choosing a series of α values corresponding to cohesive crack tips successively placed into the crack line nodes, one solves for each of them the eigenvalue $\bar{D}$ as well as the eigenmode $\bar{w}_{,\alpha}$ (approximated as a discrete eigenvector) from a discrete approximation of (34). Knowing $\bar{D}$ and $\bar{w}_{,\alpha}$, one may then simply evaluate $\bar{\sigma}_{N_u}$ from the discrete approximation of (35).

The tensile strength of the foam was determined from the tensile test without notch; $f_t' = 3.1$ MPa. Measurements of the initial slope of the load–deflection curve of the fracture specimen furnished $E = 87.0$ MPa and $v = 0.32$. The fracture energy was then determined on the basis of (34) and (35) by optimum fitting of the size effect data obtained from the present tests of edge-notched prismatic specimens in tension. Then, noting that $G_f = w_c f_t'/2$, the crack opening displacement w_c at the intersection of the linearly softening the stress–displacement law (triangular softening law) with the displacement axis was evaluated as $w_c = 2G_f/f_t'$.

It is also instructive to have the entire diagrams of the dimensionless nominal stress versus the dimensionless load–point displacement. Since the eigenvalue approach yields only the maximum loads and not the entire load–deflection diagrams, these diagrams had to be calculated using the Hillerborg–Petersson type approach; see the graphs in Fig. 11a. For the case of geometric similarity, and with the use dimensionless coordinates, the initial slopes of all the calculated diagrams in this figure must be the same. As we can see, they are indeed the same.

The calculated load–deflection curves in Fig. 11 explain the reason why the medium and large size specimens failed immediately upon reaching the peak load. These failures cannot be blamed on poor control of the test because the load–deflection diagrams for these specimens are seen to exhibit a sharp snapback, i.e., a post-peak softening with a positive slope. In the case of snapback even a perfectly stiff control of the load–point displacement cannot prevent instability. The fact that tensile notched specimen large enough to obey LEFM must exhibit a snapback was established theoretically (Bažant, 1987; Bažant and Cedolin, 1991, Chapter 12).

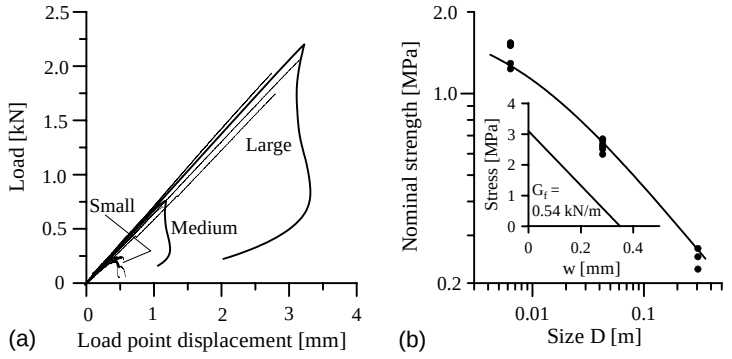

Fig. 11. (a) Load–deflection curves of edge-notched prismatic specimens specimens tested, for different specimen sizes (thin lines—the experiments, thick lines—calculated), and (b) size effect curve obtained from the eigenvalue analysis (35) and the corresponding softening law.

10. Conclusions

1. A strong size effect in the closed-cell PVC foam (Divinycell H100) is experimentally demonstrated. It agrees well with the size effect law proposed by Bažant (1984), which is based on asymptotic matching that describes a smooth transition between the asymptotic case of no size effect (characteristic of plasticity or any theory whose failure criterion is solely expressed in terms of stress or strain) and the asymptotic case of size effect of linear elastic fracture mechanics (governed by energy release).
2. The size effect law permits the fracture energy and the effective fracture process zone length of foam to be easily identified by measuring only the maximum loads of geometrically similar notched specimens of sufficiently different sizes (the geometrical shapes can be dissimilar, albeit at the cost of less simple evaluation).
3. A suitable fracture test specimen for very light foam is a tensioned prism with one edge notch at mid-length, fixed at the ends. This specimen fails purely by tensile fracture, while other specimens of light foam, such a three-point bend beams, are plagued by simultaneous compression collapse of foam cells at places of load application, which distorts the results.
4. Evaluation of the energy release function for this test specimen must take into account the effect of the lateral shift of the axial load resultant caused by rotational restraints at specimen ends. This effect is easily captured by LEFM if the end rotations canceled by rotational restraint are calculated from the stress intensity factor expression as a function of crack length.
5. Conclusions 1 and 2 are strengthened by analyzing recent Zenkert and Bäcklund's (1989) test data for the size effect on notched three-point bend specimens of a heavier foam (Divinycell H200). Fitting the results with a size effect formula yields realistic values of the fracture parameters of this foam.
6. A closed-form formula of asymptotic matching type, bridging the equivalent LEFM solution and plasticity solution (and similar to Bažant et al.'s (1999) formula for kink-band failures in fiber composites), is derived for long rectangular prismatic specimens of different widths, having holes of different diameter-width ratios. It is shown that this formula can describe both the size effect and change of geometry effect as recently measured on foam specimens by Fleck, Olurin and co-workers (2001). It cannot be claimed, however, that the formula could actually predict the maximum loads of these specimens. This remains unproven because the required asymptotic properties for a vanishing length of crack emanating from the hole, which are crucial for the asymptotic matching philosophy, are not exhibited by the handbook solution for the energy release function and are only crudely approximated by the modified energy release function developed here.
7. Compressed foam specimens with V-shaped notches (with an angle wide enough to prevent the notch faces from coming into contact) exhibit no size effect. This implies that the cell collapse at the tip of the notch must be essentially a yielding process rather than a softening damage process.
8. Finite element computations based on the cohesive crack model (with the same local tensile strength as obtained by independent tests) match the test results closely. This provides an independent verification of the use of the size effect method for measuring the fracture properties of foam.
9. The results demonstrate that the current design practice, in which the tensile failure of foam is generally predicted on the basis of strength criteria or plasticity, is acceptable only for small structural parts because it misses the size effect and lead to fracture energy G_f that is close to that obtained by fitting the data with the asymptotic formula. In the case of large structural parts, the size effect must be taken into account, especially if the foam can suffer large fatigue cracks or large damage zones prior to critical loading to failure.

Acknowledgements

Financial support under Grant ONR-N00014-91-J-1109 from the Office of Naval Research (monitored by Dr. Yapa D.S. Rajapakse and directed by Bažant) is gratefully acknowledged.

References

Bao, G., Ho, S., Suo, Z., Fan, B., 1992. The role of material orthotropy in fracture specimens for composites. International Journal of Solids and Structures 29 (9), 1105–1116.

Bažant, Z.P., 1984. Size effect in blunt fracture: Concrete, rock, metal. Journal of Engineering Mechanics ASCE 110, 518–535.

Bažant, Z.P., 1987. Snapback instability at crack ligament tearing and its implication for fracture micromechanics. Cement and Concrete Research 17, 951–967.

Bažant, Z.P., 1998. Size effect in tensile and compression fracture of concrete structures: computational modeling and design. In: Mihashi, H., Rokugo, K. (Eds.), Fracture Mechanics of Concrete Structures (Proc., 3rd Int. Conf., FraMCoS-3, held in Gifu, Japan). Aedificatio Publishers, Freiburg, Germany, pp. 1905–1922.

Bažant, Z.P., 2002. Scaling of Structural Strength. Hermes-Penton, London.

Bažant, Z.P., Brocca, M., 2000. Failure of foam core sandwiches: numerical simulation by microplane model. In: Rajapakse, Y.D., Kardomateas, G.A., Birman, V. (Eds.), Mechanics of Sandwich Structure (ASME Congress, Orlando), AMD-Vol. 245 (and AD-Vol. 62). Am. Soc. Mech. Engrs., New York, pp. 51–68.

Bažant, Z.P., Cedolin, L., 1991. Stability of Structures: Elastic, Inelastic, Fracture and Damage Theories. Oxford University Press, New York (and 2nd ed., Dover Publ. 2002).

Bažant, Z.P., Kazemi, M.T., 1990. Determination of fracture energy, process zone length and brittleness number from size effect, with application to rock and concrete. International Journal of Fracture 44, 111–131.

Bažant, Z.P., Li, Y.-N., 1995. Stability of cohesive crack model: Part II—Eigenvalue analysis of size effect on strength and ductility of structures. Journal of Applied Mechanics ASME 62, 965–969.

Bažant, Z.P., Li, Z., 1996. Zero-brittleness size-effect method for one-size fracture test of concrete. Journal of Engineering Mechanics ASCE 122 (5), 458–468.

Bažant, Z.P., Pfeiffer, P.A., 1987. Determination of fracture energy from size effect and brittleness number. ACI Materials Journal 84, 463–480.

Bažant, Z.P., Planas, J., 1998. Fracture and Size Effect in Concrete and Other Quasibrittle Materials. CRC Press, Boca Raton and London (Sections 9.2 and 9.3).

Bažant, Z.P., Kim, J.-J.H., Daniel, I.M., Becq-Giraudon, E., Zi, G., 1999. Size effect on compression strength of fiber composite failing by kink band propagation. International journal of Fracture 95, 103–141 (Special issue on In: Bažant, Z.P., Rajapakse, Y.D.S. (Eds.), Fracture Scaling).

Brocca, M., Bažant, Z.P., Daniel, I.M., 2001. Microplane model for stiff foams and finite element analysis of sandwich failure by core indentation. International Journal of Solids and Structures 38, 8111–8132.

Cottrell, A.H., 1963. Iron and Steel Institute Special Report 69, p. 281.

Fleck, N.A., Olurin, O.B., Chen, C., Ashby, M.F., 2001. The effect of hole size upon the strength of metallic and polymeric foams. Journal of the Mechanics and Physics of Solids 49, 2015–2030.

Führing, H., 1973. Approximation functions for K-factors of cracks in notches. International Journal of Fracture 9, 328–331.

Gibson, L.J., Ashby, M.F., 1997. Cellular Solids: Structure and Properties, 2nd ed. Cambridge University Press, Cambridge, UK.

Gdoutos, E.E., Daniel, I.M., Wang, K.A., 2001. Multiaxial characterization and modeling of a PVC cellular foam. Journal of Thermoplastic Composite Materials 14 (5), 365–373.

Guinea, G.V., Elices, M., Planas, J., 1997. On the initial shape of the softening function of cohesive materials. International Journal of Fracture 87, 139–149.

Hillerborg, A., 1985. Numerical methods to simulate softening and fracture of concrete. In: Sih, G.C., DiTomasso, A. (Eds.), Fracture Mechanics of Concrete: Structural Application and Numerical Calculation. Martinus Nijhoff, Dordrecht, pp. 141–170.

Hillerborg, A., Modéer, M., Petersson, P.E., 1976. Analysis of crack formation and crack growth in concrete by means of fracture mechanics and finite elements. Cement and Concrete Research 6, 773–782.

Irwin, G.R., 1958. Fracture. In: Flügge, W. (Ed.), Handbuch der Physik, vol. VI. Springer Verlag, Berlin, pp. 551–590.

Li, Y.-N., Bažant, Z.P., 1994. Eigenvalue analysis of size effect for cohesive crack model and its application. Journal of the Mechanics and Physics of Solids 41 (2), 331–350.

Li, Y.N., Liang, R.Y., 1993. The theory of eigenvalue problem in the cohesive crack model and its application. Journal of the Mechanics and Physics of Solids 41 (2), 331–350.

Murakami, Y., 1986. Stress Intensity Factors Handbook. Oxford University Press, New York.

Olurin, O.B., Fleck, N.A., Ashby, M.F., 2001. Tensile and Compressive Failure of Notched Cellular Foams. Advanced Engineering Materials 3 (1–2), 55–58.

Petersson, P.E., 1981. Crack growth and development of fracture zones in plain concrete and similar materials. Doctoral Dissertation, Lund Institute of Technology, Lund, Sweden (Sec. 13.2).

Shipsha, A., Burman, M., Zenkert, D., 2000. On mode I fatigue crack growth in foam core materials for sandwich structures. Journal of Sandwich Structures 2, 103–116.

Tada, H., Paris, P.C., Irwin, G.R., 1985. The Stress Analysis of Cracks Handbook. Del research Corp., Hellertown, PA.

Triantafillou, T.C., Gibson, L.J., 1987. Failure maps for foam core sandwich beams. Material Science and Engineering 95, 37–53.
Weibull, W., 1939. The phenomenon of rupture in solids. Proc. Royal Swedish Institute of Engineering Research, vol. 153. (Ingenioersvetenskaps Akad. Handl.), Stockholm, pp. 1–55.
Weibull, W., 1951. A statistical distribution function of wide applicability. Journal of Applied Mechanics ASME 18, 293–297.
Wells, A.A., 1961 Unstable crack propagation in metals-cleavage and fast fracture. Symposium on Crack Propagation, Cranfield, vol. 1. pp. 210–230.
Zenkert, D., 1989. PVC sandwich core materials: fracture behaviour under mode II and mixed mode loading. Materials Science and Engineering 108, 233–240.
Zenkert, D., Bäcklund, J., 1989. PVC sandwich core materials: mode I fracture toughness. Composite Science and Technology 34, 225–242.
Zi, G., Bažant, Z.P., 2003. Eigenvalue method for computing size effect of cohesive crack with residual stress, with application to kink bands in composites. International Journal of Engineering Science 41 (13–14), 1519–1534.